RSC Advances

PAPER

View Article Online
View Journal | View Issue

Cite this: *RSC Adv.*, 2021, **11**, 12153

Two dimensional Ni_2P/CdS photocatalyst for boosting hydrogen production under visible light irradiation

Li Huang,[a] Ruchao Gao,[a] Liuying Xiong,[a] Perumal Devaraji,[a] Wei Chen,[ab] Xiying Li[ab] and Liqun Mao[*ab]

Received 24th January 2021
Accepted 17th March 2021

DOI: 10.1039/d1ra00625h

rsc.li/rsc-advances

Two-dimensional (2D) semiconductor materials have attracted considerable attention in the field of photocatalysis due to the high interfacial charge separation efficiency and abundant surface active sites. Herein, we have fabricated 2D/2D sheets of Ni_2P/CdS heterostructure for photocatalytic H_2 evolution. The microscopic and photocatalytic activity results suggested that Ni_2P nanosheets were coupled with snowflake CdS. The optimal hydrogen production rate reached 58.33 mmol h^{-1} g^{-1} (QE = 34.38%, λ = 420 nm) over 5 wt% Ni_2P, which is equivalent to that of 1 wt% Pt/CdS. Compared with pure CdS, Ni_2P/CdS presented lower fluorescence intensity and stronger photocurrent density, which demonstrated that the 2D/2D Ni_2P/CdS heterojunction photocatalyst significantly improved the separation efficiency of photogenerated electrons and holes. The excellent performance of Ni_2P/CdS clearly indicated that Ni_2P was an excellent cocatalyst and could provide abundant active sites for hydrogen evolution.

1. Introduction

Since Fujishima *et al.* reported photocatalytic hydrogen production from water splitting in 1972, increasing attention has been paid in this research field,[1] and thus a large amount of photocatalysts have been developed, among which CdS is thought of as a promising photocatalytic semiconductor material with high conductivity and narrow band gap.[2] Due to the fast recombination of photo-induced carriers and severe photocorrosion, CdS alone is inactive,[3] and always works with noble metal cocatalysts, such as Pt, Pd, Ru, *etc.*, which has significantly increased the cost of catalysts and thus limits their application.[4] Recently, many non-precious metal co-catalysts have been developed,[5] such as metal sulfide,[6–8] metal carbide,[9,10] metal nitride,[7,11] metal phosphide[12–14] and metallic oxide.[15,16] To promote the activity of CdS photocatalysts, our group has tried several strategies, including: (1) Pt-based bimetal cocatalysts, such as PtPd NPs,[17] PtNi NPs,[18] and PdNi NPs,[19] which can not only reduce the use of precious metals, but also improve the photocatalytic performance because of the synergistic effect of the bimetals; (2) nobel metal free cocatalysts, such as Ni[20] or Co,[21] also display high photocatalytic activity of H_2 generation; (3) structure redesign, such as $PtNi_x$ polyhedra,[22] $PtNi_x$ hollow structures[23] and $PtNi_xCo_y$ concave nanocubes,[24] which provide more active sites for photocatalytic H_2 generation, and result in the promotion of activity of CdS; (4) dealloying $PtNi_x$ as a cocatalyst, which shows even higher activity in photocatalytic hydrogen generation.[25]

In this work, a 2D/2D Ni_2P/CdS heterostructure was synthesized and used in photocatalytic hydrogen generation from water splitting under visible light. Transition metal phosphates are widely concerned by researchers because of their availability, cheap price and simple preparation method.[26] Due to the "ensemble effect" of phosphorus, the binding strength of hydrogen is moderate, which is of great significance for photocatalytic hydrogen production.[27] Therefore, 2D structured Ni_2P was prepared as the cocatalyst, and modified on the surface of CdS nanosheet to form a novel 2D/2D Ni_2P/CdS heterojunction, which shows excellent performance of photocatalytic hydrogen production, and provides a promising prospect for large-scale production of hydrogen in the future.

2. Experimental section

2.1 Reagents and materials

All the chemical reagents, including $(NH_4)_2SO_3 \cdot H_2O$ were procured from Alfa Aesar Co. Led, China. $Cd(CH_3COO)_2 \cdot 4H_2O$ and HF were procured from Haohua Chemical Reagent Co. Ltd, China. $Ni(CH_3COO)_2 \cdot 4H_2O$, and NH_2CSNH_2 were ordered from Kermel Chemical Reagent Co. Ltd, China. $C_2H_8N_2$ was procured from Damao Chemical Reagent Co. Ltd, China. $NiCl_2 \cdot 6H_2O$ and red phosphorus were procured from aladdin Chemical Reagent Co. Ltd, China, and used without any further purification.

[a]*Henan Engineering Research Center of Resource & Energy Recovery from Waste, Henan University, Kaifeng 475004, PR China. E-mail: mlq@henu.edu.cn; Tel: +86-13513781969*

[b]*Institute of Functional Polymer Composites, College of Chemistry and Chemical Engineering, Henan University, Kaifeng 475004, PR China*

2.2 Synthesis of photocatalysts

Synthesis procedure of CdS. Snow-flake CdS was prepared by a typical hydrothermal method.[28] Briefly, 5 mmol $Cd(CH_3COO)_2 \cdot 4H_2O$, 6 mmol $CS(NH_2)_2$, 0.805 mL 40 wt% HF and 79.2 mL deionized water were added into a 100 mL Teflon-lined autoclave and allowed to stir for 1 h at room temperature, followed by heating in an oven at 473 K for 20 h. After the autoclave cooled down naturally, the product was washed with deionized water and ethanol for several times. The resultant precipitate was dried in a vacuum oven at 343 K for 12 h.

Synthesis procedure of Ni_2P. Ni_2P was synthesized by a facile solvothermal method with red phosphorus and $Ni(CH_3COO)_2 \cdot 4H_2O$ used as phosphorus and nickel source, respectively. Firstly, 0.023 mol of red phosphorus was mixed with 15 mL of deionized water and 15 mL of ethylenediamine. After stirring for 30 min, it was transferred into a 50 mL Teflon-lined autoclave, and was kept at 373 K for one hour. Subsequently, it was cooled naturally before 0.004 mol of nickel acetate was added, and was kept still for 12 h at 413 K. After it was cooled down naturally, the precipitate was collected by centrifugation and dried at 333 K overnight in vacuum oven.

Synthesis procedure of Ni_2P/CdS. A calculated amount of Ni_2P was added to the distilled water stirred for 30 minutes to disperse well, then mixed with CdS and stirred evenly, and finally modified on the surface of CdS by photocatalytic deposition. The Ni_2P/CdS photocatalyst with an x wt% loading Ni_2P loaded is called x wt% Ni_2P/CdS. A simple schematic diagram of Ni_2P/CdS synthesis was shown in Fig. 1.

2.3 Characterization

XRD patterns were obtained by X-ray diffraction (XRD; Bruker, Germany) with Cu-Kα radiation in 2θ range of 5–90° at a scan rate of 0.3°/s. Scanning electron microscopy (SEM) images were obtained using a JEOL 7610F (Japan). Transmission electron microscopy (TEM) as well as high resolution transmission electron microscopy (HR-TEM) images were collected using a JEM-2010 electron microscope equipped with selected area electron diffraction (SAED). The ultraviolet-visible (UV-vis) diffuse reflectance spectra (DRS) were measured by a UV-vis spectrophotometer UV-2600 (Shimadzu, Japan), The photoluminescence (PL) emission spectra were acquired with a fluorescence spectrophotometer (FLS 980, UK).

2.4 Electrochemical measurements

All electrochemical measurements were recorded on a CHI-760 electrochemical system equipped with a standard 3-electrode system and 50 mL of 0.5 M Na_2SO_4 as electrolyte solution. A glassy carbon electrode (3 mm diameter, 0.07 cm^2) was used as the working electrode for Linear sweep voltammetry (LSV), and the modified FTO plates were used as the working electrode for photocurrent spectroscopy test and Mott–Schottky test. A platinum (Pt) wire and a Ag/AgCl were used as the counter and the reference electrodes for all the electrochemical tests, respectively. The measurement of electrochemical impedance spectroscopy (EIS) was conducted at 5 mV AC (alternating current) voltage with a frequency range of 1–10^5 Hz. A 300 W Xenon lamp with a 420 nm was used as the light source.

2.5 Evaluation of photo–catalytic activity

A Teflon-lined stainless steel cylindrical reactor with a circulating water jacket was used as the photoreactor for H_2 generation *via* photocatalytic water splitting. The diameter of the photoreactor is 12.5 cm, and there is a round quartz glass window (with a diameter of 7 cm) on the top center of the

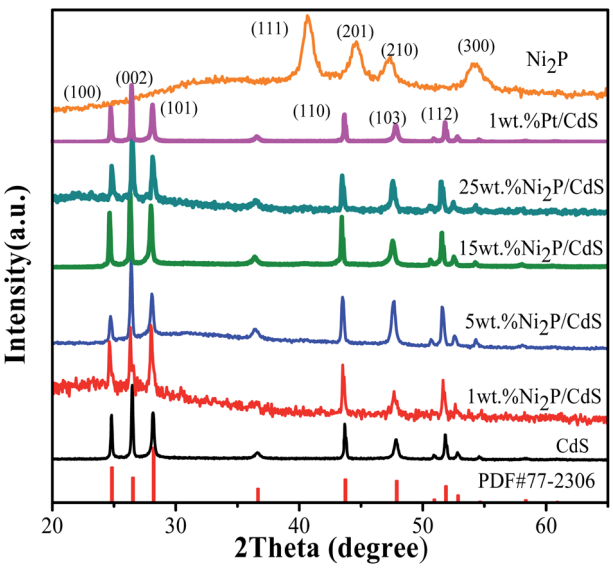

Fig. 2 XRD patterns of CdS, Ni_2P, Pt/CdS and Ni_2P/CdS with various Ni_2P loading contents.

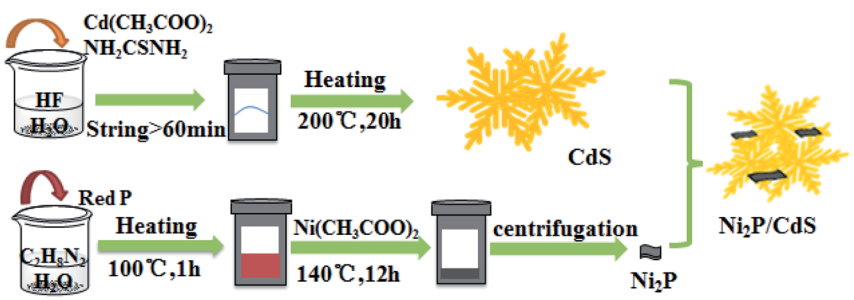

Fig. 1 Schematic illustration of the synthesis process of Ni_2P/CdS photocatalyst.

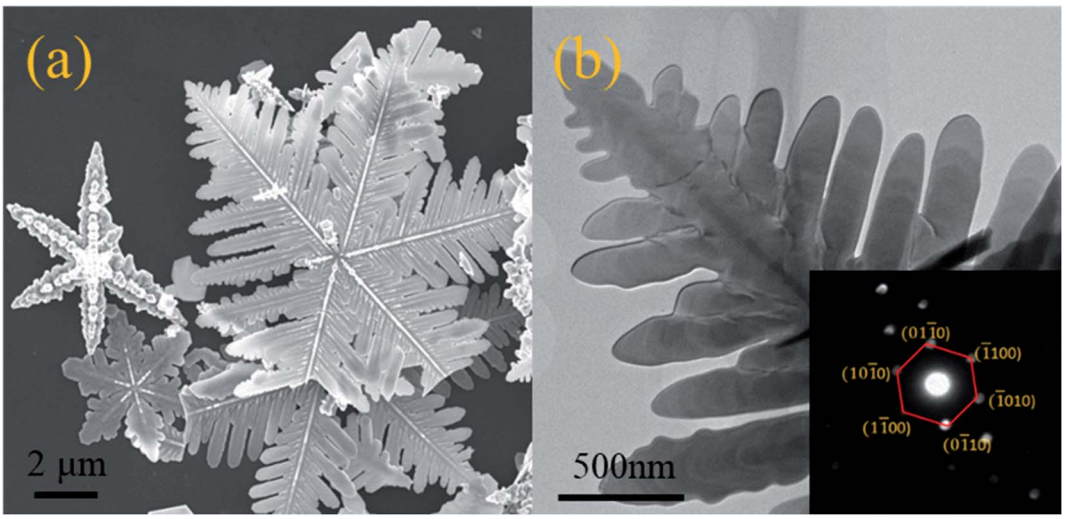

Fig. 3 SEM image (a), TEM image and insert SAED pattern (b) of as-prepared CdS.

photoreactor. A 300 W Xenon lamp was used as the light source with a 420 nm cut-off filter and the measured illumination area of light is approximately 38 cm^2. For photocatalytic H_2 generation reaction, 0.05 g of CdS photocatalyst and certain amount of Ni_2P were added to 50 mL of 1.5 M aqueous $(NH_4)_2SO_3 \cdot H_2O$ (sacrificial agent) solution. High purity

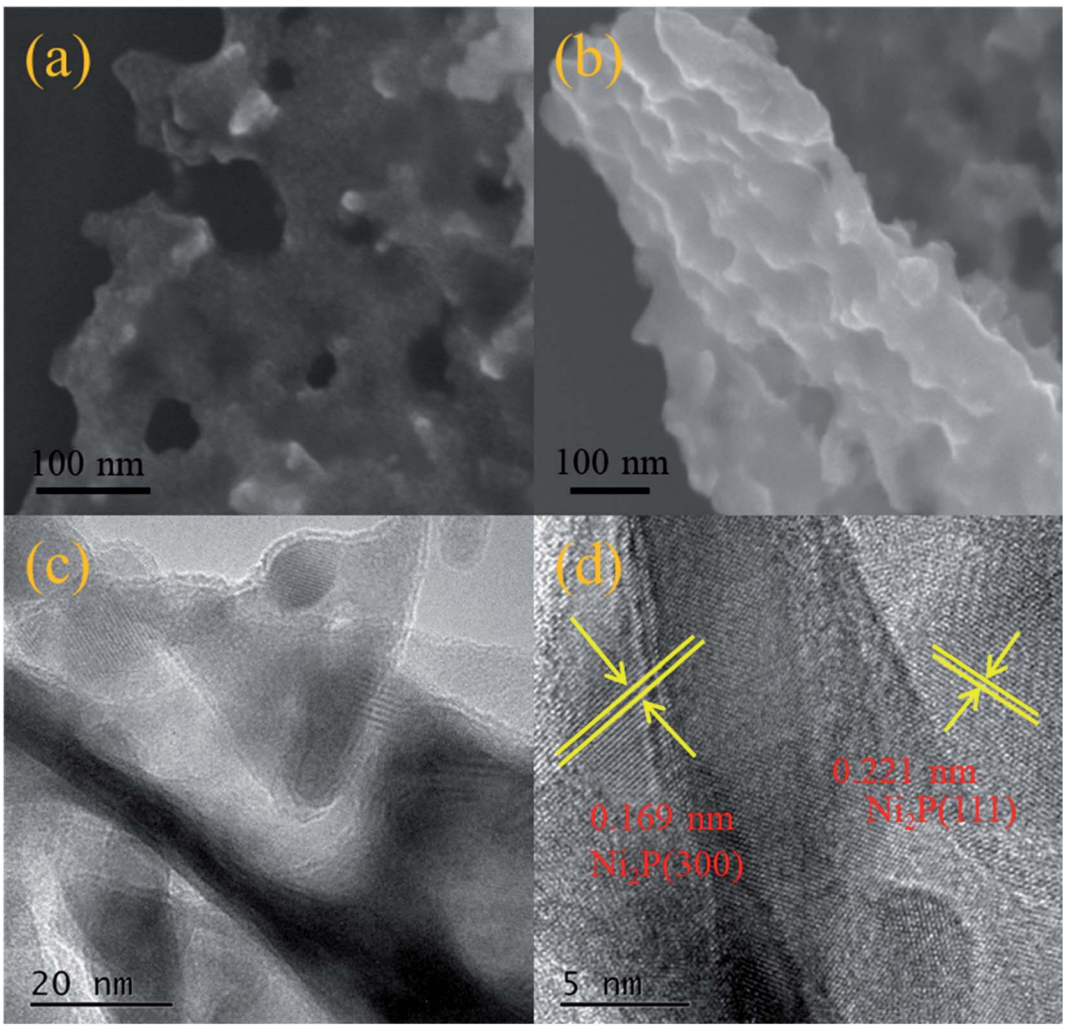

Fig. 4 SEM images (a and b), HRTEM images (c and d) of Ni_2P, respectively.

nitrogen was pumped for 30 minutes before photocatalytic activity reaction to obtain an air isolation. Furthermore, the quantum efficiency (QE) of the samples were tested and can be calculated as:

$$\mathrm{QE} = \frac{\text{the number of evolved hydrogen atoms}}{\text{the number of incident photons}} \times 100\%$$

3. Results and discussion

3.1 Structure and morphology

Fig. 2 shows the XRD patterns of CdS, co-catalyst Ni_2P, Ni_2P/CdS and Pt/CdS photocatalyst. It can be seen that the CdS shows several main diffraction peaks at 24.84°, 26.53°, 28.30°, 43.94° and 47.91°, corresponding to (100), (002), (101), (110) and (103) crystal surfaces, respectively (PDF#77-2306). The main peaks of Ni_2P at 40.74°, 44.61°, 47.36°, and 54.20° match well with (111), (201), (210), and (300) planes, respectively, which illustrates that the Ni_2P cocatalyst is successfully prepared by the solvothermal method.[29]

As mentioned in the Experimental section, Ni_2P or Pt NPs were deposited on the surface of CdS by its photo-induced electrons during the photocatalytic hydrogen generation reaction. After that, Ni_2P/CdS or Pt/CdS were separated from the reaction solution, dried at 343 K and the as-obtained powders were used for XRD analysis. As shown in Fig. 2, the XRD patterns of Ni_2P/CdS and Pt/CdS are consistent with that of CdS, and no diffraction peak are observed for Ni_2P, which may be attributed to the low loading amount of Ni_2P.

Fig. 3 shows the SEM, TEM and SAED of CdS respectively. As shown Fig. 3(a), the snowflake structure of CdS with a diameter of ~10 μm was confirmed by both SEM and TEM. Every snowflake structure of CdS has 6 main crystal axes with an angle of 60°, and the secondary crystal axes appear along the main crystal axis, forming many dendrites. The angle between the secondary and primary crystal axes is also 60°. The SAED images (Fig. 3(b), in the inset) of CdS show many bright and highly ordered diffraction pots, which implies the presence of single crystal structure. In the images of calibrated SAED, the six crystal faces corresponding to the inner diffraction points are $(01\bar{1}0)$, $(\bar{1}100)$, $(\bar{1}010)$, $(0\bar{1}10)$, $(1\bar{1}00)$, $(10\bar{1}0)$, indicating that the

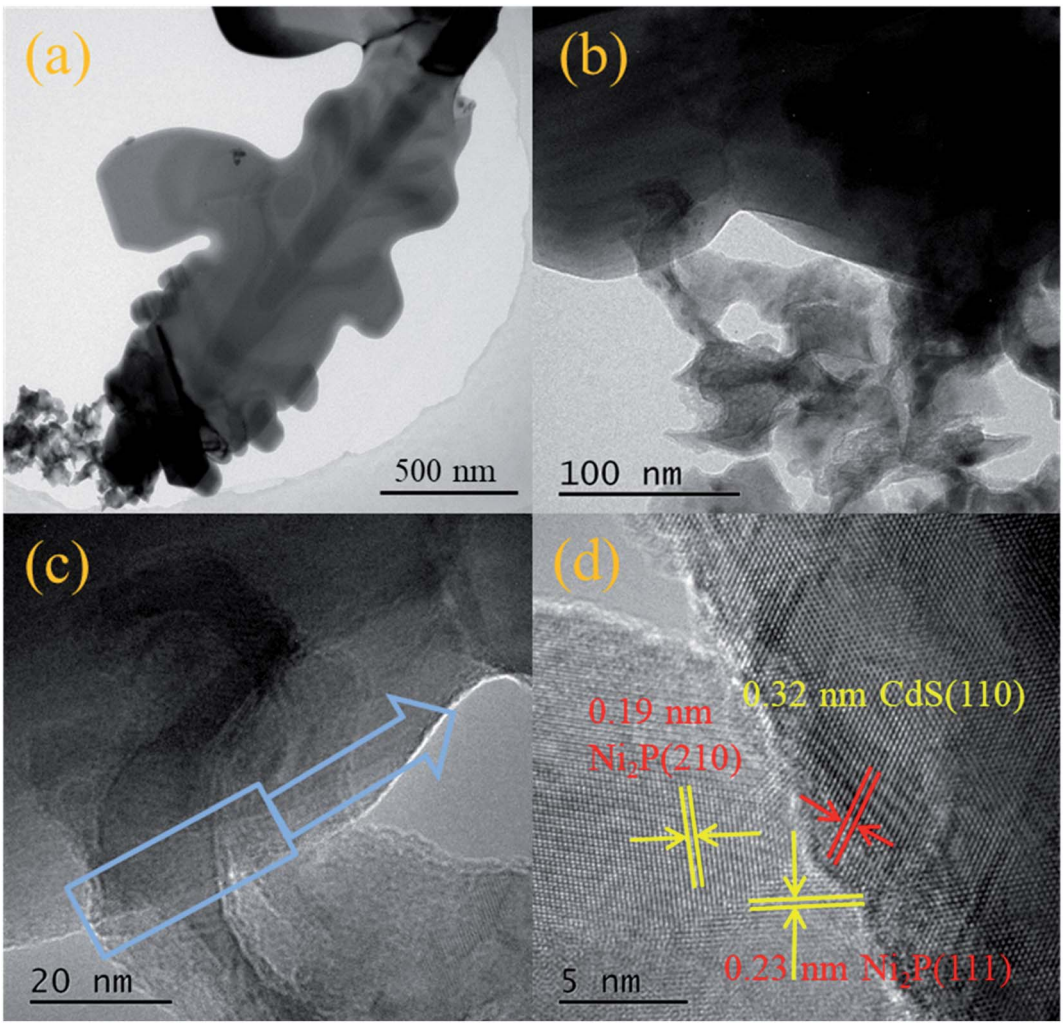

Fig. 5 HRTEM images (a–d) of 5 wt% Ni_2P/CdS.

CdS is hexagonal, which is consistent with XRD results. Combined with the XRD test results, it is suggested that HF was adsorbed on the surface (0001) in the hydrothermal reaction process to inhibit the growth of crystals in the vertical direction, leading to the formation of CdS flake structure. The crystals grew rapidly to form the primary crystals, meanwhile the lateral crystals grew out to form a snowflake like structure.

The SEM images (Fig. 4(a) and (b)) show that Ni_2P possesses ultrathin nanosheets structure with irregular pores. The HR-TEM images (Fig. 4(c) and (d)) further reveal the subtle nanosheet structure of Ni_2P with the crystal plane spacing of 0.221 nm and 0.169 nm, attributed to the (111) and (300) crystal planes, respectively (PDF#74-135).[30]

Fig. 5 displays TEM images (Fig. 5(a) and (b)) and the HR-TEM images (Fig. 5(c) and (d)) of Ni_2P/CdS, respectively. The interplanar spacing of Ni_2P nanosheets was calculated to be 0.22 nm and 0.19 nm, corresponding to its (111) and (210) plane, respectively. In addition, a *d*-spacing of 0.32 nm was clearly seen and attributed to the (110) plane of CdS.[31] Most importantly, the presence of the heterojunction between Ni_2P and CdS was confirmed by Fig. 5. The heterointerface generated in Ni_2P/CdS will promote the transfer of photogenerated charge carriers to the surface, and inhibit the recombination of photogenerated e^-–h^+ pairs, result in high the photocatalytic activity.

3.2 Photocatalytic hydrogen generation action

Under visible light irradiation ($\lambda \geq 420$ nm), the photocatalytic H_2 evolution of the prepared samples were performed by using 1.5 M as $(NH_4)_2SO_3 \cdot H_2O$ as the sacrificial reagent. Fig. 6(a) displays H_2 evolution performance of Ni_2P/CdS photocatalyst with different Ni_2P loading contents. CdS alone shows the low activity, probably due to the fast recombination of photogenerated carriers. On the contrary, CdS coupled with Ni_2P significantly promoted the hydrogen generation rate. In particular, the highest H_2 generation activities reached 58.33 mmol g^{-1} h^{-1} (QE = 34.38%, λ = 420 nm) with 5 wt% Ni_2P/CdS. However, Ni_2P/CdS showed poor photocatalytic activity at low loading amounts of Ni_2P, possibly because of less active sites and the heterogeneous junction interface of Ni_2P/CdS. When Ni_2P loading amounts increased up to 25 wt%, the hydrogen production rate of Ni_2P/CdS was lowered than that of pure CdS, because the excess Ni_2P nanosheets would affect the light absorption and utilization of CdS. Furthermore, the activity of Ni_2P/CdS was also compared with Pt/CdS photocatalyst. In terms of our previous study, the photocatalytic H_2 evolution activity of 1wt% Pt/CdS with the best loading amounts was evaluated under the same photocatalytic system.[32] As shown in Fig. 6(b), the hydrogen production rate of 5 wt% Ni_2P/CdS is colsed to that of 1 wt% Pt/CdS, indicating that Ni_2P is an excellent hydrogen evolution co-catalyst and expected to be a desirable substitute for noble metal Pt.

In order to investigate the hydrogen production stability of Ni_2P/CdS, the 5 wt% Ni_2P/CdS catalyst was evaluated for cyclic hydrogen production. At the beginning of each cycle, 2 mL deionized water and 5 g $(NH_4)_2SO_3 \cdot H_2O$ were used as the supplement. Fig. 7(a) displays the 4 continuous experiments, and the corresponding photocatalytic hydrogen production rate is shown in Fig. 7(b). It can be seen that the hydrogen production activity of 5 wt% Ni_2P/CdS is remained basically unchanged after 20 h of cyclic experiments. The four cycle experiments show that hydrogen production rates of 5 wt% Ni_2P/CdS are 57.1, 56.2, 55.7 and 54.5 mmol g^{-1} h^{-1}, respectively, and there is no significant decrease in photocatalytic evolution. The result indicates that 5 wt% Ni_2P/CdS catalyst possesses excellent stability under long time light irradiation.

3.3 Spectral properties

Fig. 8(a) shows the UV-visible diffuse reflection spectrum of the as-prepared samples. It can be seen from the graph that the absorption band edge of CdS is located at around 525 nm in the visible light region, indicating that CdS has a good visible light absorption capacity. When Ni_2P was modified on the CdS surface, the absorption of Ni_2P/CdS photocatalyst enhanced

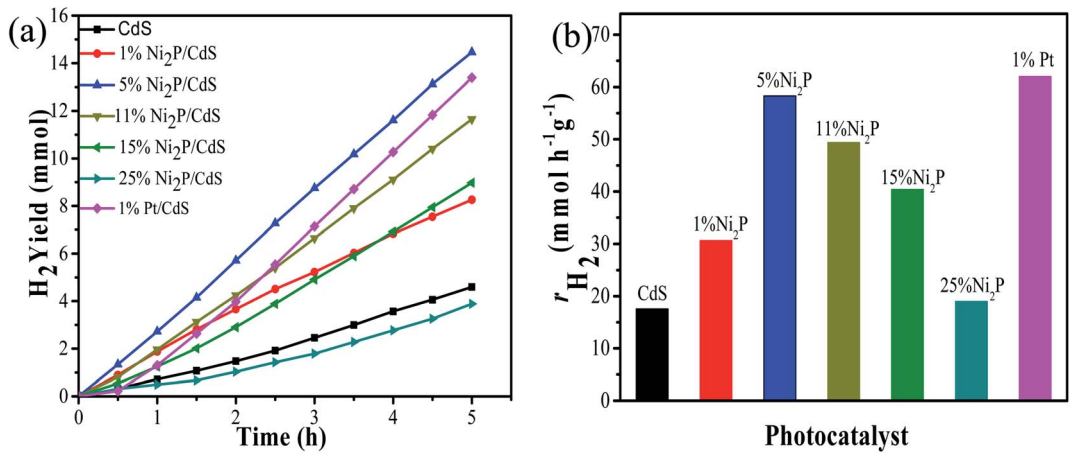

Fig. 6 (a) Time-dependent photocatalytic H_2 evolution and (b) average rate of H_2 evolution over Ni_2P/CdS with various Ni_2P loading contents. Reaction conditions: A 300 W Xe lamp equipped with a cut-off filter ($\lambda \geq 420$ nm), 50 mL 1.5 mol L^{-1} (10.0613 g/50 mL) $(NH4)_2SO_3 \cdot H_2O$ aqueous solution, 0.05 g Ni_2P/CdS photocatalyst.

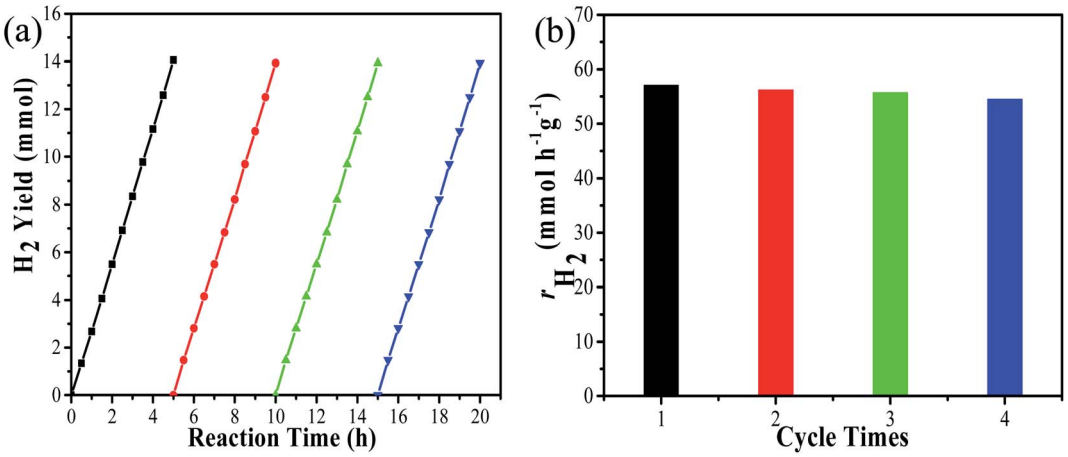

Fig. 7 Photocatalytic hydrogen evolution stability for 5 wt% Ni_2P/CdS. (a) Time-dependent photocatalytic H_2 evolution and (b) average rate of H_2 evolution. Reaction conditions: A 300 W Xe lamp equipped with a cut-off filter ($\lambda > 420$ nm), 50 mL 1.5 mol L^{-1} (10.0613 g/50 mL) $(NH_4)_2SO_3 \cdot H_2O$ aqueous solution, 0.05 g Ni_2P/CdS photocatalyst.

significantly. According to the Tauc plots of CdS and Ni_2P shown in Fig. 8(b), the bandgap of CdS and Ni_2P were calculated to be 2.41 eV and 1.31 eV, respectively. Combined with Mott–Schottky test results, the energy levels and positions of CdS and Ni_2P could be analyzed. As shown in Fig. 8(c and d), the slopes of both curves are positive, which demonstrated that CdS and Ni_2P are typical n-type semiconductors. The flat-band potential (V_{fb}) of CdS and Ni_2P are measured to be −0.79 eV and −0.35 eV

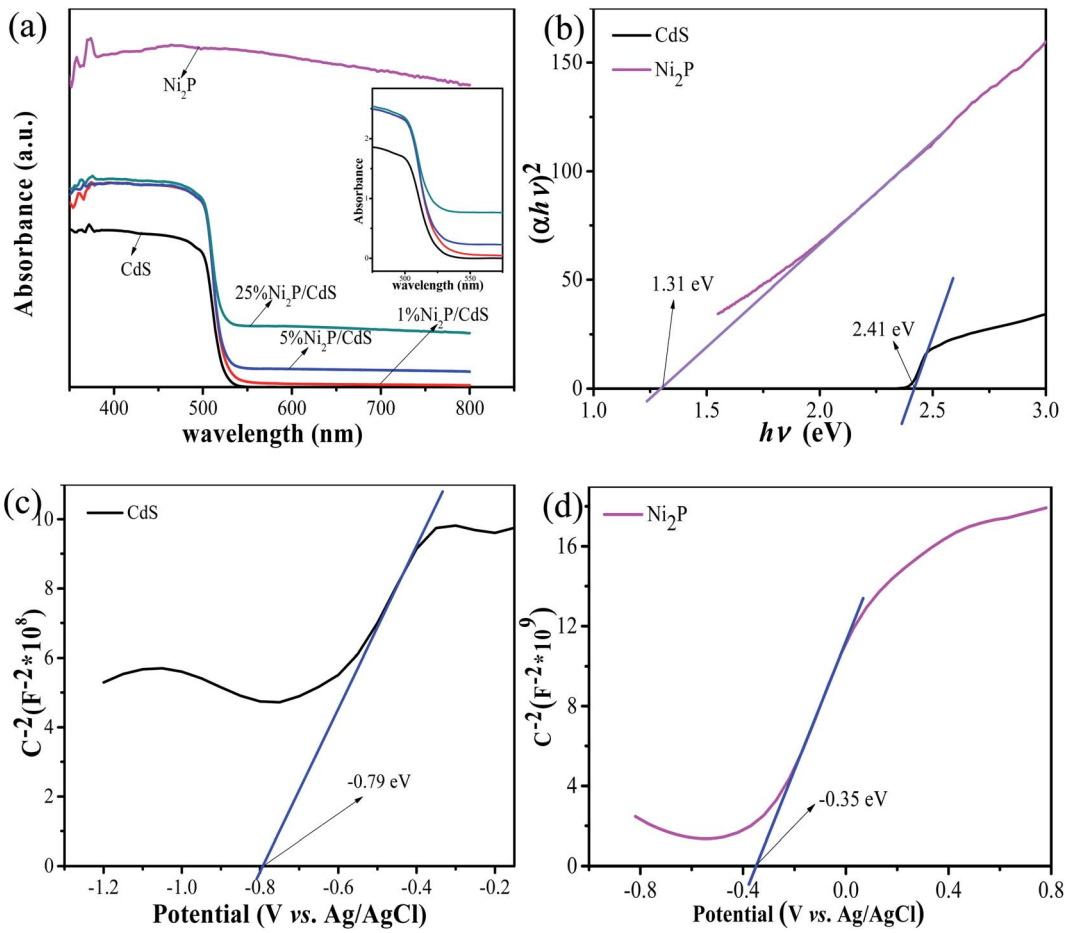

Fig. 8 Ultraviolet-visible diffuse reflectance spectra of CdS, Ni_2P/CdS photocatalyst (a), Tauc plots of CdS, Ni_2P (b), (c) Mott–Schottky plot of CdS and (d) Mott–Schottky plot of Ni_2P.

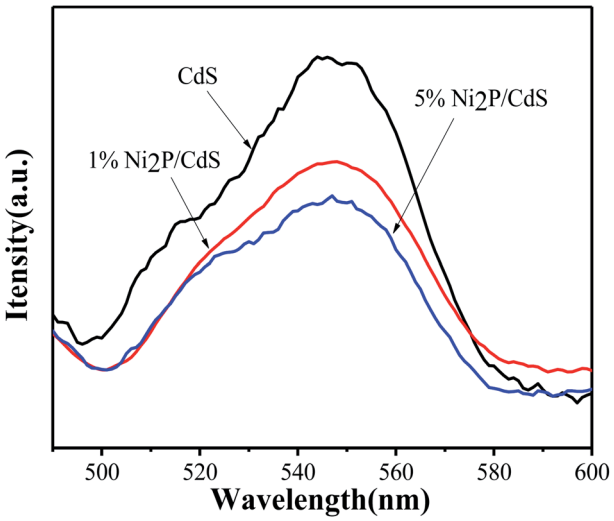

Fig. 9 Photoluminescence spectra of CdS and Ni_2P/CdS photocatalyst.

vs. Ag/AgCl, respectively, and the corresponding standard hydrogen electrodes are −0.59 eV and −0.15 eV ($E_{NHE} = E_{Ag/AgCl}$ + 0.2). Based on the literature reports,[33] the conduction band (E_{CB}) of n-type semiconductor is very close to the measured V_{fb} value. In n-type semiconductors, V_{fb} is 0.1–0.2 eV higher than that of E_{CB}, therefore, E_{CB} of CdS and Ni_2P were estimated to be −0.69 eV and −0.25 eV *vs.* NHE, respectively. According to the formula of $E_{VB} = E_{CB} + E_g$, the valence band potentials of CdS and Ni_2P can be calculated as 1.72 eV and 1.06 eV *vs.* NHE, respectively, which are basically consistent with the results reported in the literatures.[34]

Since the recombination of photogenerated electron–hole pairs in semiconductors can produce fluorescence, the steady PL spectra could be used to evaluate the separation ability of photoelectron–hole pairs.[35] It can be seen from the figure that pure CdS shows the highest fluorescence emission characteristics, indicating its highest photogenic carrier recombination rate. When 1 wt% Ni_2P was introduced into the system, the emission intensity decreased significantly and fluorescence quenching occurred. Further increase up to 5 wt% Ni_2P in photocatalytic system would further weaken the fluorescence intensity. The results show that the 2D/2D heterostructure formed between CdS and Ni_2P can greatly promote electron transfer rate and improve the photocatalytic activity (Fig. 9).

3.4 Electrochemical measurements

Fig. 10 displays the LSV curves of CdS, Ni_2P/CdS photocatalyst and its corresponding Tafel curves measured in 0.5mol L^{-1} Na_2SO_4 electrolyte solution. It can be seen from Fig. 10(a) that

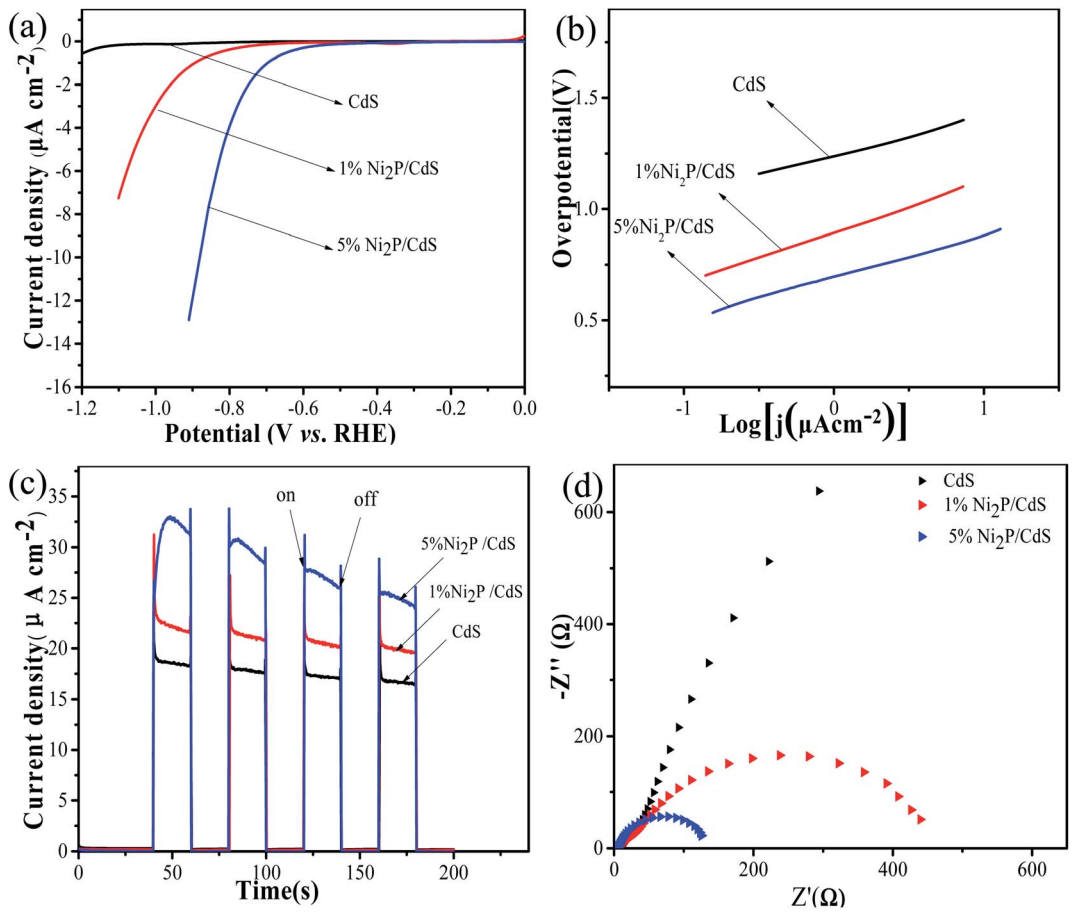

Fig. 10 Linear sweep voltammetry (LSV) curves (a), corresponding tafel plots (b), photocurrent–time curves (c) and EIS spectra (d) of CdS, Ni_2P/CdS photocatalyst, respectively.

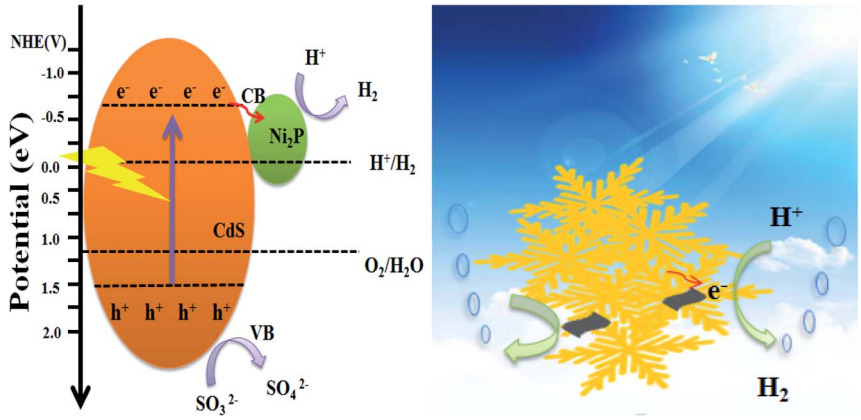

Fig. 11 The proposed photocatalytic mechanism for Ni_2P/CdS photocatalyst.

Ni_2P can significantly improve the hydrogen evolution current density after being modified on the CdS surface, thus showing better hydrogen evolution performance. By comparing with the Tafel curves of CdS, 1 wt% Ni_2P/CdS and 5 wt% Ni_2P/CdS (Fig. 10(b)), Ni_2P nanosheets loaded on CdS shows lower overpotential at any current density. The above results can also be confirmed by transient photocurrent experiments (i–t) under visible light irradiation. As shown in Fig. 10(c), photocurrent is generated immediately at the moment of illumination, indicating that the sample can be illuminated by a xenon lamp to generate photoelectrons, which transferred to the electrode to generate photocurrent. Compared with bare CdS, the photocurrent density of Ni_2P/CdS increases significantly, which suggests that the 2D–2D Ni_2P/CdS can effectively separate photogenerated electrons and holes to improve the photocatalytic reaction efficiency. Additionally, EIS can evaluate the rate of carrier transport on the semiconductor material surface. As shown in Fig. 10(d), the semicircular diameter is the smallest when Ni_2P nanosheets modified on the surface of CdS, which verifies that the 2D/2D Ni_2P/CdS heterojunction has the lowest charge transfer resistance and thus shows outstanding performance of photocatalytic H_2 production.[36]

On the basis of the above experimental results and analysis, Fig. 11 proposes the possible mechanism of Ni_2P as the co-catalyst supported on CdS surface to promote the photocatalytic activity under visible light irradiation. CdS and Ni_2P Mott–Schottky test results show that E_{CB} of CdS and Ni_2P is −0.59 eV and −0.15 eV *vs.* NHE, and E_{VB} is 1.72 eV and 1.06 eV *vs.* NHE, respectively. Since the E_{CB} of CdS is more negative than that of Ni_2P, the photogenerated electrons will be transferred to Ni_2P surface across the intimate interface, then reduce H^+ to H_2. At the same time, the holes on the valence band of CdS are rapidly consumed by the sacrificial reagents. The matching band position of CdS and Ni_2P provides an effective and rapid transmission direction for photogenerated electrons and holes, and thus improves the separation efficiency of photogenerated carriers. According to the performance of Ni_2P/CdS on photocatalytic H_2 production, Ni_2P has been demonstrated to behave similar as the noble metal co-catalysts, which can quickly capture electrons, promote separation efficiency of photocatalyst carriers, and improve the efficiency of photocatalytic water splitting. What's more, 2D/2D heterojunction between CdS and Ni_2P reduces the transfer distance of photogenerated charge carries to the material surface, which is conducive to the transport and separation of photocatalytic carriers.

4. Conclusion

In this paper, the preparation of 2D/2D structure Ni_2P/CdS and hydrogen production have been studied. The results show that the special 2D/2D structure is conducive to the separation of the photogenerated electrons from holes and significantly enhanced the rate of hydrogen evolution. According to the activity data, 5 wt% Ni_2P/CdS exhibited the optimal hydrogen production rate of 58.33 mmol h^{-1} g^{-1} (QE = 34.38%, λ = 420 nm). The stability test displayed that the activity of 5 wt% Ni_2P/CdS decreased by only 4.55% after 4 cycles of photocatalytic H_2 evolution, indicating that the synthesized 2D/2D Ni_2P/CdS heterojunction has the robust and highly stable performance in the photocatalytic hydrogen production under long time visible light irradiation. SEM and HRTEM characterization showed the micron flake-like single crystal structure of CdS, the nanosheet structure of Ni_2P, and the heterojunction formed between the interfaces of Ni_2P and CdS. PL and I–T test results showed that 5 wt% Ni_2P/CdS displayed lower fluorescence intensity and higher photocurrent density compared with pristine CdS, which suggested that the Ni_2P/CdS photocatalyst with 2D/2D structure was more favorable for the separation of photogenerated e^-–h^+ pairs. Based on the study in this paper, we concluded the reason of high performance H_2 production as follows: firstly, as an effective co-catalyst for hydrogen evolution, Ni_2P can quickly capture electrons, promote the separation efficiency of photogenerated carriers and photocatalytic performance; secondly, the special 2D/2D contact between CdS and Ni_2P is favorable to the transmission of photogenerated electrons and inhibit the recombination of photogenerated carries. In summary, this work displays a possible way to construct 2D/2D heterostructure materials with high

photocatalytic performance, which will stimulate tremendous interest in further exploration.

Conflict of interest

Authors have no conflict of interest to declare.

Acknowledgements

This work was supported by the Natural Science Foundation of Henan Province (182300410246).

References

1 A. Fujishima and K. Honda, *Nature*, 1972, **238**, 37–38.
2 L. Cheng, Q. Xiang, Y. Liao and H. Zhang, *Energy Environ. Sci.*, 2018, **11**, 1362–1391.
3 D. C. Yong-Jun Yuan, Z.-T. Yu and Z.-G. Zoub, *J Mater Chem A*, 2013, **6**, 11606–11630.
4 X. Zou and Y. Zhang, *Chem. Soc. Rev.*, 2015, **44**, 5148–5180.
5 J.-R. Ran, J. Zhang, J.-G. Yu, M. Jaroniec and S.-Z. Qiao, *Chem. Soc. Rev.*, 2014, **43**, 7787–7812.
6 J.-T. Zhao, P. Zhang, J. J.-. Fan, J.-H. Hu and G.-S. Shao, *Appl. Surf. Sci.*, 2018, **430**, 466–474.
7 R. Kumar, D. Das and A. K. Singh, *J. Catal.*, 2018, **359**, 143–150.
8 K. Zhang, M. Fujitsuka, Y. Du and T. Majima, *ACS Appl. Mater. Interfaces*, 2018, **10**, 20458–20466.
9 Z. Sun, Z. Yu, Y. Liu, C. Shi, M. Zhu and A. Wang, *J. Colloid Interface Sci.*, 2019, **533**, 251–258.
10 Y.-Y. Zhao, J. Guo, A.-M. Liu and T.-L. Ma, *J. Colloid Interface Sci.*, 2020, **814**, 152271.
11 R. Boppella, J. Tan, W. Yang and J. Moon, *Adv. Funct. Mater.*, 2018, **29**, 1807976.
12 D. P. Kumar, J. Choi, S. Hong, D. A. Reddy, S. Lee and T.-K. Kim, *ACS Sustainable Chem. Eng.*, 2016, **4**, 7158–7166.
13 Q.-H. Liang, L.-X. Zhong, C.-F. Du, Y.-B. Luo, J. Zhao, Y. Zheng, J. Xu, J. Ma, C. Liu, S. Li and Q. Yan, *ACS Nano*, 2019, **13**, 7975–7984.
14 Q.-Y. Jian, X.-Q. Hao, Z.-L. Jin and Q.-X. Ma, *Phys. Chem. Chem. Phys.*, 2020, **22**, 1932–1943.
15 M. Benamira, N. Doufar and H. Lahmar, *Preparation of ZrO_2–Fe_2O_3 Nanoparticles and Their Application as Photocatalyst for Water Depollution and Hydrogen Production*, Springer, Singapore, 2021, pp. 11–18.
16 M. Benamira, H. Lahmar, L. Messaadia, G. Rekhila, F. Z. Akika, M. Himrane and M. Trari, *Int. J. Hydrogen Energy*, 2020, **45**, 1719–1728.
17 X.-Y. Li, H. Liu, S. Liu, J. Zhang, W. Chen, C.-P. Huang and L.-Q. Mao, *Int. J. Hydrogen Energy*, 2016, **41**, 23015–23021.
18 L.-Q. Mao, Q.-Q. Ba, S. Liu, X.-J. Jia, H. Liu, W. Chen and X.-Y. Li, *RSC Adv.*, 2018, **8**, 31529–31537.
19 Q.-Q. Ba, X.-J. Jia, L. Huang, X.-Y. Li, W. Chen and L.-Q. Mao, *Int. J. Hydrogen Energy*, 2019, **44**, 5872–5880.
20 H. Wang, W. Chen, J. Zhang, C.-H. Huang and L.-Q. Mao, *Int. J. Hydrogen Energy*, 2015, **40**, 340–345.
21 W. Chen, Y. Wang, M. Liu, L. Gao, L.-Q. Mao, Z.-Y. Fan and W.-F. Shangguan, *Appl. Surf. Sci.*, 2018, **444**, 485–490.
22 L.-Q. Mao, Q.-Q. Ba, X.-J. Jia, S. Liu, H. Liu, J. Zhang, X.-Y. Li and W. Chen, *RSC Adv.*, 2019, **9**, 1260–1269.
23 Q.-Q. Ba, X.-J. Jia, L. Huang, X.-Y. Li, L. Gao and L.-Q. Mao, *Int. J. Hydrogen Energy*, 2019, **44**, 28104–28112.
24 X.-J. Jia, S. Liu, L. Huang, P. Devaraji, L. Walekar, W. Chen, X.-Y. Li, S. Liu and L.-Q. Mao, *Catal. Sci. Technol.*, 2020, **10**, 113–123.
25 X.-J. Jia, Q.-Q. Ba, L. Huang, P. Devaraji, W. Chen, X.-Y. Li and L.-Q. Mao, *Int. J. Hydrogen Energy*, 2019, **44**, 26169–26180.
26 N. Xiao, S.-S. Li, X.-L. Li, L. Ge, Y.-Q. Gao and N. Li, *Chin. J. Catal.*, 2020, **41**, 642–671.
27 P. Liu and J. A. Rodriguez, *J. Am. Chem. Soc.*, 2005, **127**, 14871–14878.
28 C.-X. Li, L.-J. Han, R.-G. Liu, H.-H. Li, S.-J. Zhang and G.-G. Zhang, *J. Mater. Chem.*, 2012, **22**, 23815.
29 E. J. Popczun, J. R. McKone, C. G. Read, A. J. Biacchi, A. M. Wiltrout, N. S. Lewis and R. E. Schaak, *J. Am. Chem. Soc.*, 2013, **135**, 9267–9270.
30 T. Liu, A. Li, C.-B. Wang, W. Zhou, S.-J. Liu and L. Guo, *Adv. Mater.*, 2018, **30**, e1803590.
31 J.-J. Fang, Y.-K. Chen, W. Wang, L. Fang, C.-H. Lu, C. Zhu, J. Kou, Y. Ni and Z. Xu, *Appl. Catal., B*, 2019, **258**, 117762.
32 W. Chen, S. Liu, T.-T. Chu, Q.-Q. Ba, X.-X. Jia and L.-Q. Mao, *Chem. Res.*, 2018, **29**, 233–240.
33 M. Bo, J.-P. Zhao, Z.-H. Ge, Y.-Y. Chen and Z.-H. Yuan, *Sci. China Mater.*, 2019, **63**, 258–266.
34 H. An, X.-Y. Yan, H. Li, B.-L. Yang, J.-J. Wei and G.-D. Yang, *ACS Appl. Energy Mater.*, 2019, **2**, 4195–4204.
35 C.-D. Nguyen, V.-H. Nguyen, L. M. T. Pham and T.-Y. Vu, *Int J Hydrog Energy*, 2020, **45**, 15063–15075.
36 H.-L. Li, J.-Q. Pan, W.-J. Zhao and C.-R. Li, *Appl. Surf. Sci.*, 2019, **497**, 143769.